Molecular insights into substrate recognition and catalysis by tryptophan 2,3-dioxygenase

Molecular insights into substrate recognition and catalysis by tryptophan 2,3-dioxygenase

Farhad Forouhar*, J. L. Ross Anderson†, Christopher G. Mowat†, Sergey M. Vorobiev*, Arif Hussain*, Mariam Abashidze*, Chiara Bruckmann†, Sarah J. Thackray†, Jayaraman Seetharaman*, Todd Tucker*, Rong Xiao‡, Li-Chung Ma‡, Li Zhao‡, Thomas B. Acton‡, Gaetano T. Montelione‡, Stephen K. Chapman†, and Liang Tong*§

*Department of Biological Sciences, Northeast Structural Genomics Consortium, Columbia University, New York, NY 10027; †School of Chemistry, University of Edinburgh, West Mains Road, Edinburgh EH9 3JJ, United Kingdom; and ‡Center for Advanced Biotechnology and Medicine and Northeast Structural Genomics Consortium, Rutgers University, Piscataway, NJ 08854

Communicated by Wayne A. Hendrickson, Columbia University, New York, NY, November 13, 2006 (received for review September 25, 2006)

Tryptophan 2,3-dioxygenase (TDO) and indoleamine 2,3-dioxygenase (IDO) constitute an important, yet relatively poorly understood, family of heme-containing enzymes. Here, we report extensive structural and biochemical studies of the *Xanthomonas campestris* TDO and a related protein SO4414 from *Shewanella oneidensis*, including the structure at 1.6-Å resolution of the catalytically active, ferrous form of TDO in a binary complex with the substrate L-Trp. The carboxylate and ammonium moieties of tryptophan are recognized by electrostatic and hydrogen-bonding interactions with the enzyme and a propionate group of the heme, thus defining the L-stereospecificity. A second, possibly allosteric, L-Trp-binding site is present at the tetramer interface. The sixth coordination site of the heme-iron is vacant, providing a dioxygen-binding site that would also involve interactions with the ammonium moiety of L-Trp and the amide nitrogen of a glycine residue. The indole ring is positioned correctly for oxygenation at the C2 and C3 atoms. The active site is fully formed only in the binary complex, and biochemical experiments confirm this induced-fit behavior of the enzyme. The active site is completely devoid of water during catalysis, which is supported by our electrochemical studies showing significant stabilization of the enzyme upon substrate binding.

cancer | heme enzymes | immunomodulation | indoleamine 2,3-dioxygenase

Tryptophan 2,3-dioxygenase (TDO) and indoleamine 2,3-dioxygenase (IDO) catalyze the oxidative cleavage of the L-tryptophan (L-Trp) pyrrole ring, the first and rate-limiting step in L-Trp catabolism through the kynurenine pathway (1–3). In addition, IDO has been implicated in a diverse range of physiological and pathological conditions, including suppression of T cell proliferation, maternal tolerance to allogenic fetus, and immune escape of cancers (4–8), and is an attractive target for drug discovery against cancer and autoimmune and other diseases (2, 9–12).

Despite catalyzing identical biochemical reactions (Fig. 1*a*), the sequence similarity between TDO and IDO is extremely low. An alignment of their sequences is only possible based on their structures, which suggests a sequence identity of 10% between them (Fig. 1*b*). In comparison, *Xanthomonas campestris* TDO shares 34% sequence identity with human TDO (Fig. 1*b*), demonstrating the remarkable evolutionary conservation of this enzyme. TDO is a homotetrameric enzyme and is highly specific for L-Trp and related derivatives such as 6-fluoro-Trp as the substrate. In comparison, IDO is monomeric, and shows activity toward a larger collection of substrates, including L-Trp, D-tryptophan (D-Trp), serotonin, and tryptamine (3), although the K_m for D-Trp is ≈100-fold higher than that for L-Trp (13). The structure of human IDO in the catalytically inactive, ferric [Fe(III)]-heme state in complex with the 4-phenylimidazole inhibitor has recently been reported (14). Although this structure gave information about important active site residues, the inhibitor is coordinated to the heme iron and does not provide any information regarding Trp or oxygen binding.

To provide direct insight into substrate recognition and catalysis by these enzymes, we report here the crystal structures at up to 1.6-Å resolution of the active, reduced (Fe(II)) TDO from *X. campestris* in a binary complex with the substrate L-Trp or 6-fluoro-Trp. Our structures reveal for the first time the structural basis for the stereospecificity of this important enzyme. Our structural information is confirmed by biochemical studies and offers significant molecular insight into tryptophan dioxygenation by TDO and IDO.

Results

Structure Determination. Crystals of the reduced (Fe(II)) TDO from *X. campestris* in a binary complex with the substrate L-Trp or 6-fluoro-Trp were obtained after extensive efforts and by using anaerobic conditions, because the oxidized (Fe(III)) enzyme has much lower affinity for L-Trp (see below). The structures at up to 1.6-Å resolution of these binary complexes [Table 1; and see supporting information (SI) Table 3] as well as that of the free enzyme were determined by molecular replacement based on the structure of the apo enzyme, in the absence of heme, which we had determined by the selenomethionyl single-wavelength anomalous diffraction method (PDB entry 1YW0) (15).

The structure of the SO4414 protein from *Shewanella oneidensis* (16) was determined at 2.4-Å resolution by molecular replacement based on our structure of the apo enzyme (PDB entry 1ZEE).

Structure of TDO. The structure of *X. campestris* TDO monomer contains 12 helices (named αA through αL) and no β-strands (Figs. 1*b* and 2*a*). TDO is an intimately associated tetramer (Fig. 2*b*), and ≈4,500 Å^2 of the surface area of each monomer is buried in the tetramer. Helices αB and αC are located in the extensive, mostly hydrophobic interface between two of the monomers. The N-terminal segments (residues 21–40, including helix αA) of the two monomers are swapped in this dimer (Fig.

Author contributions: F.F., J.L.R.A., and C.G.M. contributed equally to this work; F.F., J.L.R.A., C.G.M., G.T.M., S.K.C., and L.T. designed research; F.F., J.L.R.A., C.G.M., S.M.V., A.H., M.A., C.B., S.J.T., J.S., T.T., R.X., L.-C.M., L.Z., and T.B.A. performed research; F.F., J.L.R.A., C.G.M., S.M.V., A.H., M.A., C.B., S.J.T., J.S., R.X., L.-C.M., T.B.A., G.T.M., S.K.C., and L.T. analyzed data; and F.F., J.L.R.A., C.G.M., T.B.A., G.T.M., S.K.C., and L.T. wrote the paper.

The authors declare no conflict of interest.

Abbreviations: D-Trp, D-tryptophan; IDO, indoleamine 2,3-dioxygenase; L-Trp, L-tryptophan; TDO, tryptophan 2,3-dioxygenase.

Data deposition: The atomic coordinates have been deposited in the Protein Data Bank, www.pdb.org (PDB ID codes 1YW0, 2NW7, 2NW8, 2NW9, 1ZEE, and 2NWB).

§To whom correspondence should be addressed. E-mail: ltong@columbia.edu.

This article contains supporting information online at www.pnas.org/cgi/content/full/0610007104/DC1.

BIOCHEMISTRY

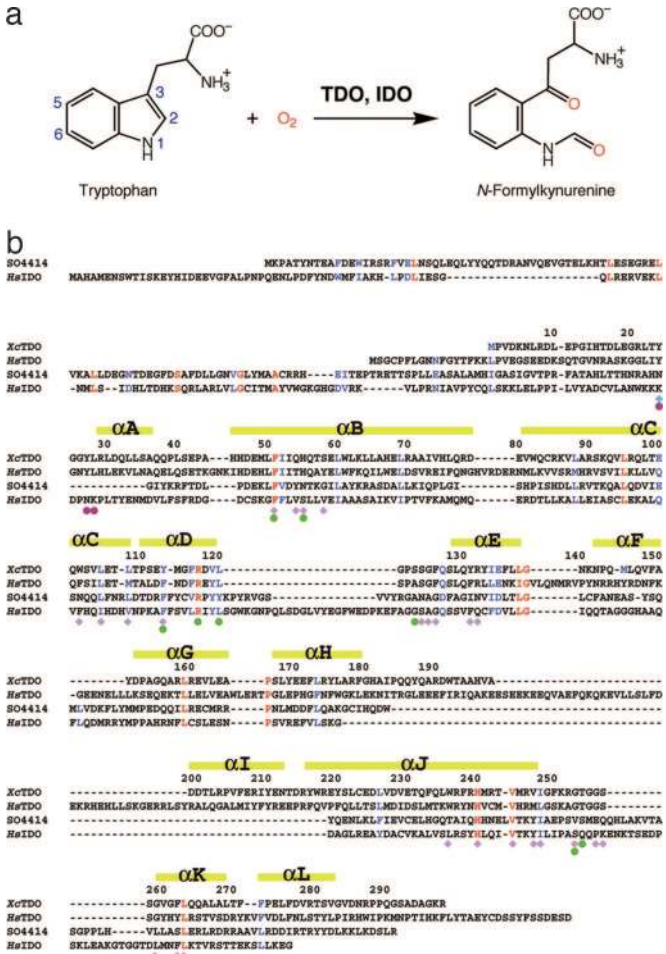

Fig. 1. Primary structures of TDO and IDO. (*a*) The biochemical reaction catalyzed by TDO and IDO. (*b*) Amino acid sequence alignment of *X. campestris* TDO (*Xc*TDO), human TDO (*Hs*TDO), *S. oneidensis* SO4414 (SO4414), and human IDO (*Hs*IDO). The filled circles indicate residues involved in binding L-Trp, and the diamonds indicate residues involved in binding heme. The symbols for residues before helix αA are given different colors, to indicate that they are from another monomer of the tetramer.

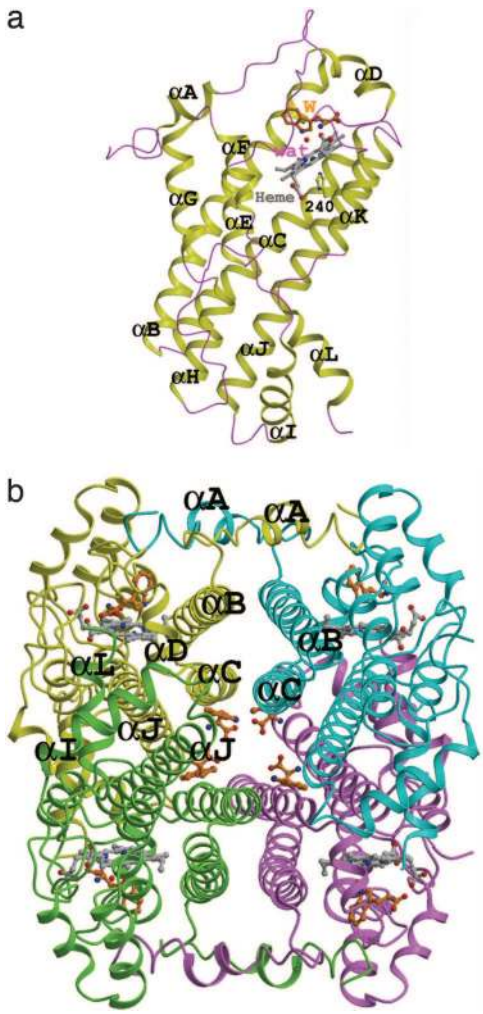

Fig. 2. The structure of TDO. (*a*) Schematic representation of the structure of the monomer of *X. campestris* TDO. The α-helices are shown in yellow and labeled. Heme is shown in gray, and L-Trp is shown in orange (labeled W). The water molecule is shown as a red sphere (labeled wat). (*b*) Schematic representation of the tetramer of *X. campestris* TDO. The four monomers are colored in yellow, cyan, violet, and green. Helices in the tetramer interface are labeled. The Trp molecules in the tetramer interface are also shown. Produced with Molscript (35) and rendered with Raster3D (36).

2*b*), which is important for the catalysis by TDO because several residues in this segment are part of the binding site for the Trp residue in the active site (see below).

Binding Mode of the L-Trp Substrate to TDO. Our structure of the binary complex defines the molecular mechanism for the recognition of the L-Trp substrate by TDO. Clear electron density was observed for heme and L-Trp in the active site based on the crystallographic analysis at 1.6-Å resolution (Fig. 3*a*). The L-Trp substrate is located in a pocket over the distal face of the heme, having interactions with residues in helices αB and αD, and the αD–αE and αJ–αK loops (Figs. 1*b* and 3*b*). The carboxylate group of Trp is recognized by bidentate ion-pair interactions with the side chain of Arg 117 (in helix αD). The carboxylate group is also hydrogen-bonded to the side chain hydroxyl of Tyr113 (helix αD) and the main chain amide of Thr 254 (αJ-αK loop). The ammonium ion of L-Trp is recognized by the 7-propionate side chain of the heme group (Fig. 3*b*), and it is also hydrogen-bonded to the side chain hydroxyl of Thr 254. The indole ring is located ≈3.5 Å above and perpendicular to the heme and is held in place by van der Waals interactions with the side chains of Phe 51 (helix αB) and several other hydrophobic residues, including Tyr 24, Tyr 27, and Leu 28 from the N-terminal segment of another monomer of the tetramer (Fig. 3*b*). In addition, the N1 nitrogen of the indole ring is hydrogen-bonded to the side chain of His 55 (helix αB) (Fig. 3*b*).

A water molecule is present in the active site of this binary complex (Fig. 3*a*), hydrogen-bonded to the ammonium ion of L-Trp and the main-chain amide of residue Gly 125 (Fig. 3*b*). The water is 3.5 Å from the ferrous atom in the heme, too far for ligating interactions. The iron atom is still 0.3 Å out of the plane of the heme, on the side of the proximal His 240 ligand (SI Fig. 5).

The crystal was exposed to a solution saturated with nitric oxide (NO) before being flash-frozen, but we did not observe the binding of this dioxygen analog in the structure. This is confirmed by our structure of the binary complex with 6-fluoro-Trp, which was not exposed to NO but contained the same density for the water molecule (SI Fig. 6). The structure of the 6-fluoro-Trp binary complex is essentially identical to that of the L-Trp binary complex (SI Fig. 6). NO probably dissociated from the heme during the cryofreezing manipulations in the anaerobic box.

Induced-Fit Behavior of TDO. Our structural information suggests that TDO is an induced-fit enzyme. Although the active site

Table 1. Summary of crystallographic information

Protein	TDO (holoenzyme)	TDO (holoenzyme)	TDO (holoenzyme)	TDO (apoenzyme)	SO4414 (holoenzyme)	SO4414 (apoenzyme)
Ligand	L-Trp	6-fluoro-Trp	None	None	None	None
Maximum resolution, Å	1.6	1.8	2.7	2.7	2.4	2.3
R_{merge}, %*	6.9 (52.7)	8.6 (60.9)	13.0 (32.3)	16.6 (74.0)	10.4 (63.0)	6.6 (30.6)
Beam line	ESRF BM14	ESRF BM14	NSLS X4A	APS 21BM	NSLS X4A	NSLS X4A
Completeness, %	87 (65)	87 (61)	72 (54)	82 (68)	83 (60)	87 (71)
R factor, %†	17.1 (18.9)	16.6 (17.9)	25.7 (25.7)	25.0 (32.1)	21.7 (23.5)	23.4 (26.7)
Free R factor, %	18.9 (22.0)	18.4 (21.1)	26.3 (26.2)	29.4 (35.1)	22.5 (24.1)	27.5 (31.5)
rms deviation in bond lengths, Å	0.005	0.005	0.008	0.011	0.007	0.006
rms deviation in bond angles, °	1.0	1.0	1.2	1.6	1.1	1.0
Most-favored region, %	92	91	89	86	92	91

*$R_{merge} = \Sigma_h\Sigma_i|I_{hi}-\langle I_h\rangle|/\Sigma_h\Sigma_i I_{hi}$. The numbers in parentheses are for the highest-resolution shell.
†$R = \Sigma_h|F_h^o - F_h^c|/\Sigma_h F_h^o$.

pocket is well defined in the binary complex (Fig. 3*b*), the αJ–αK loop, which helps to form the walls of this pocket, is disordered in the free enzyme, and the αD-αE loop has a somewhat different conformation (Fig. 3*c*; and see SI Fig. 7). Moreover, the Arg 117 side chain assumes a different conformation in the free enzyme (Fig. 3*c*). Upon recognition of the L-Trp substrate, a complex and extensive network of interactions is established (Fig. 3*b*), thus stabilizing the active site region. Although this region is exposed to the solvent in the free enzyme, it is completely shielded from the solvent in the binary complex, and only the carboxylate group of the 6-propionate of heme is visible on the surface.

Additional evidence for the induced-fit behavior is observed in the active site of the second TDO monomer in the asymmetric unit. The binding mode of the L-Trp substrate is very different in this monomer (Fig. 3*d*; and see SI Fig. 7). The Trp side chain is not positioned as deeply into the pocket, and the hydrogen bond between the ring nitrogen and the side chain of His 55 is lost (distance of 3.8 Å). Both nitrogen atoms are instead hydrogen-bonded to a water molecule, located 3.5 Å from the heme iron but at a position distinct from that of the water in the active site of the other monomer (Fig. 3*d*). This conformation may also be stabilized by crystal packing interactions, as the 7-propionate of heme is ion-paired with an Arg residue from another TDO tetramer in the crystal. The main chain atoms of the Trp substrate appear to be disordered, because no clear electron density was observed for them (Fig. 3*e*). Consistent with this finding, the αJ–αK loop is disordered in this molecule, similar to that in the free enzyme (Fig. 3*d*). This complex may represent an initial stage in the formation of the Michaelis complex of TDO. Proper positioning of the L-Trp substrate for catalysis would lead to the recognition of its main chain atoms and the ordering of the αJ–αK loop.

Implications for Substrate Binding by IDO. Our structure of the binary complex of TDO also has significant implications for substrate recognition by the IDOs. The rms distance for 201 structurally equivalent Cα atoms between TDO and the large domain of human IDO (PDB entry 2D0T) (14) is 3.1 Å (SI Fig. 8), calculated with the program Dali (17). Despite sharing only 10% overall sequence identity, key active-site residues are similar in TDO and IDO (Fig. 1*b*; and see SI Table 4), and L-Trp may have the same binding mode to the active site of IDO (SI Fig. 9). Ionic interactions that are important for recognizing the L-Trp ammonium ion and carboxylate group are conserved in IDO (Arg 231 and 7-propionate), explaining why L-Trp is a much better substrate than D-Trp for IDO. At the same time, hydrogen-bonding interactions to these atoms may be absent in IDO, because Tyr 113 of TDO is replaced by Phe 226 in IDO (SI Fig. 9), and the Thr 254 residue may not have an equivalent in IDO because the αJ–αK loop, disordered in the IDO structure (SI Fig. 9) (14), has highly divergent sequences in IDO compared with TDO (Fig. 1*b*). Therefore, IDO may have weaker interactions with tryptophan, which may be the reason why it cannot completely distinguish among the indoleamine substrates.

The structure comparison explains why 1-methyltryptophan is a micromolar inhibitor of IDO (18) but is essentially inactive against TDO (10). The N1 atom is directly hydrogen-bonded to the His 55 side chain in TDO (Fig. 3*b*), and its methylation will cause steric clash with this residue. In comparison, His 55 is replaced by Ser 167 in IDO (SI Table 4), which creates a small pocket that can accommodate the 1-methyl group (SI Fig. 9).

Structural similarity is also observed with the SO4414 protein from *S. oneidensis* (SI Fig. 8) (16), with an rms distance of 4.4 Å for 206 equivalent Cα atoms, suggesting that SO4414 may also be a dioxygenase. Moreover, the structure contains an extra domain that is formed by residues at the N terminus, similar to the small domain in human IDO (SI Fig. 8). In contrast to human IDO, SO4414 is a tetramer but with a different organization compared with that of TDO (SI Fig. 10). Our biochemical efforts so far have not been able to demonstrate IDO (or TDO) activity for this protein, suggesting that SO4414 may prefer a different substrate for oxygenation.

A Model for the Michaelis Complex. To help provide further insight into the catalysis by these enzymes, we built a model for the Michaelis complex, by placing one oxygen atom (O1) of the dioxygen substrate directly over the heme iron, at a distance of 2.1 Å (Fig. 4*a*). The distal oxygen atom (O2) was placed such that the O1–O2 bond is parallel to the C2–C3 bond of indole ring, giving a Fe–O1–O2 angle of 135°. This conformation places the O2 atom within 0.5 Å of the water molecule observed in our structure (Fig. 4*a*), suggesting that this water should be ejected from the active site upon dioxygen binding. The active site is therefore completely devoid of solvent molecules in this Michaelis complex.

The modeled dioxygen-binding mode reveals the activation mechanism of this substrate for the reaction. It has been established that TDO has an ordered catalytic cycle in which the protein first binds L-Trp to the ferrous form, and then binding of dioxygen is facilitated, and nucleophilic attack from the substrate C3 is initiated (3, 13, 19). In the model, the distal oxygen atom interacts with the L-Trp ammonium moiety and the backbone amide nitrogen of Gly 125 (Fig. 4*a*). The Lewis acidity

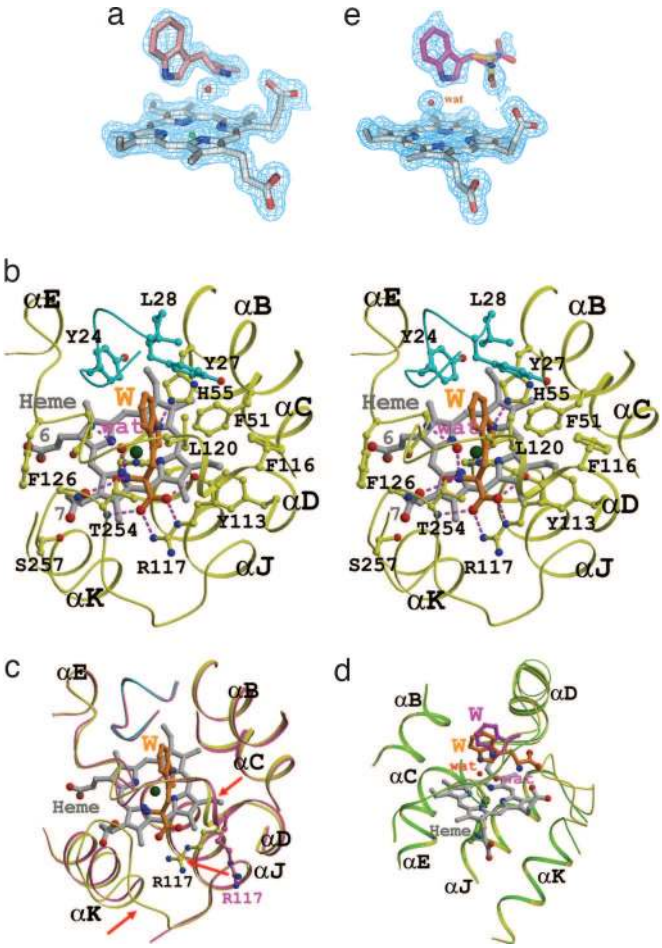

Fig. 3. Molecular basis for substrate recognition by TDO. (*a*) Final $2F_o-F_c$ electron density at 1.6-Å resolution for heme, L-Trp, and a water in the active site. Contoured at 1σ. (*b*) Stereo drawing showing the active site of *X. campestris* TDO in the binary complex with L-Trp. The segment in cyan is from another monomer of the tetramer. Hydrogen-bonding interactions are indicated with dashed lines in magenta. (*c*) Overlay of the structures of the free enzyme (in orchid) and the binary complex (yellow and cyan) in the active-site region. Regions of conformational differences are indicated with the red arrows. (*d*) Overlay of the active-site region of the second monomer (in green) and that of the first monomer (in yellow). Only the side-chain atoms of Trp are shown in the second monomer (in magenta). (*e*) Final $2F_o-F_c$ electron density at 1.6-Å resolution for heme, L-Trp, and a water in the active site of the second TDO molecule in the crystal. Contoured at 1σ. Two conformations for the main chain atoms are shown, but neither fit the density well. For the stereo version of *c* and *d*, please see SI Fig. 7. Produced with Molscript (35) and rendered with Raster3D (36).

of the hydrogen-bonding donors, coupled with the electron-withdrawing nature of the heme, would increase the electrophilicity of the bound dioxygen and render it more susceptible to nucleophilic attack by the substrate C3 atom. The increased hydrophobicity of the active site upon the exclusion of water would also aid the stabilization of an oxyferrous species. Studies with heme oxygenase suggest that the hydrogen-bonding interactions to the dioxygen substrate may also help to prevent its heterolysis (20), and the exclusion of water probably removes a hydrogen-bond competitor to the dioxygen. After the initial attack by the C3 atom, the reaction may proceed via a Criegee rearrangement or a dioxetane intermediate (SI Fig. 11). In the model, the O1–O2 atoms are in a trans configuration relative to the C2–C3 atoms of L-Trp (Fig. 4*a*), which may favor the Criegee rearrangement pathway (SI Fig. 11) (19). The Criegee pathway is also favored based on chemical, thermodynamic, and quantum mechanical considerations (3).

Our model for the Michaelis complex shows that the O1 atom is 2.6 Å from the N1 atom of L-Trp and therefore can act as the general base to extract the proton from the N1 atom (SI Fig. 11) (19). The N1 atom is hydrogen-bonded to His 55 in TDO. However, our biochemical studies show that the k_{cat} of TDO is relatively insensitive to pH over the range examined (pH 6 to pH 8) (Fig. 4*b*), and the H55A mutant had only a 10-fold decrease in the k_{cat} (Table 2), suggesting that this residue is not essential for catalysis, consistent with its replacement with a Ser residue in IDO. On the other hand, the K_m shows a marked increase at lower pH (Fig. 4*b*), probably because of the protonation of this residue.

An Allosteric Binding Site in the Tetramer Interface. We also observed the binding of four L-Trp residues to an allosteric site in the interface of the tetramer (Fig. 2*b*), with well defined electron density (SI Fig. 12). The L-Trp residue appears to be recognized specifically by the enzyme in this pocket (SI Fig. 12). There have been reports of allosteric activation by the substrate L-Trp (21, 22), and our observations offer a possibility for this effector site. Unfortunately, our kinetic studies so far have not shown any allosteric effects with *X. campestris* TDO. This site is not occupied in the 6-fluoro-Trp complex, possibly because of the lower concentration of this compound in the crystallization solution.

Biochemical Studies Confirm the Structural Observations. *X. campestris* TDO has robust catalytic activity toward L-Trp and 6-fluoro-Trp but is inactive toward D-Trp, tryptamine or indolepropionic acid (Table 2), confirming its designation as a TDO. In fact, D-Trp is a weak, competitive inhibitor of the enzyme at high concentrations (Table 2). Our binding data show that D-Trp has much lower affinity for the enzyme than L-Trp (Table 2), consistent with our structural information and explaining why D-Trp cannot be oxygenated by TDO.

The biochemical studies also provide direct evidence for the induced-fit behavior of TDO. There is a large increase in the affinity of the enzyme for L-Trp when the heme iron is reduced (K_d [ferric Fe(III) heme] = 3.8 mM, whereas K_d [ferrous Fe(II) heme] = 4.1 μM) (Table 2). The electrochemistry data show a large, positive shift in reduction potential (+136 mV) in the presence of 15 mM L-Trp (Fig. 4*c*). In fact, the shift in reduction potential almost perfectly correlates with the increase in affinity for L-Trp on reduction, both giving an estimated $\Delta\Delta G$ of 15 kJ/mol. These data show that there is a significant stabilization of the ferrous form when substrate is bound. This stabilization could also play a physiological role to keep the protein reduced, and therefore active, when L-Trp is present.

Our structural studies have defined the binding mode of the substrate L-Trp to TDO, revealing the structural basis for the stereospecificity of this important enzyme. The induced-fit behavior of TDO, confirmed by our biophysical studies, appears crucial for the exclusion of water from the active site and for stabilizing the enzyme in the presence of the substrates. Finally, structural comparisons among these enzymes reveal the striking evolutionary conservation of the heme-dependent dioxygenases.

Materials and Methods

The experimental protocols are summarized here. More detailed information can be found in *SI Materials and Methods*.

Protein Expression and Purification. Full-length *X. campestris* TDO (NESG ID XcR13) and *S. oneidensis* SO4414 (NESG ID SoR52) were cloned into a pET-21d (Novagen, San Diego, CA) derivative, with a C-terminal hexahistidine tag, and overexpressed at 17°C in *Escherichia coli* BL21(DE3) pMGK cells. Hemin (7 μM

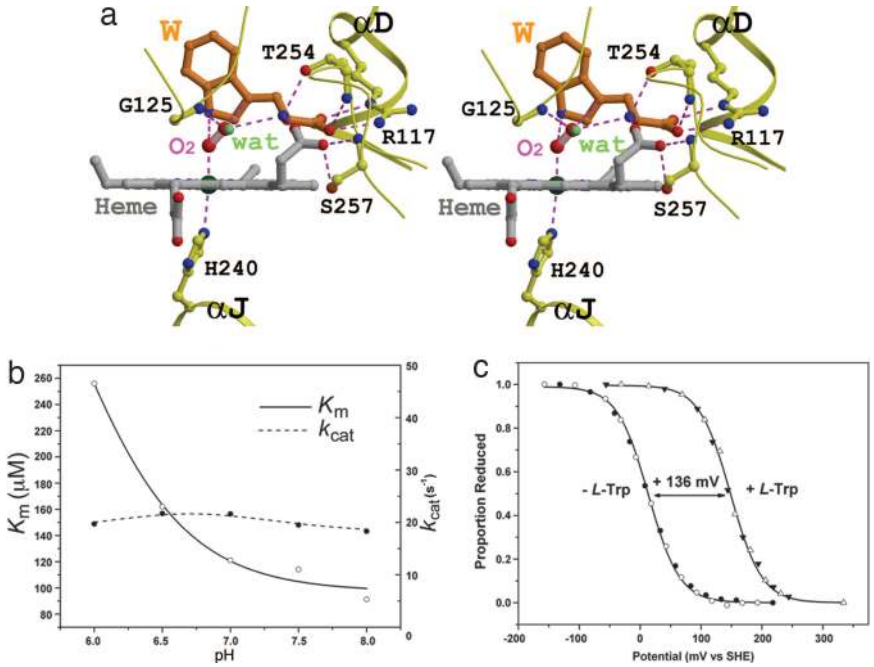

Fig. 4. Molecular insights into the catalysis by TDO. (*a*) Model of the Michaelis complex. The water molecule is shown as a small sphere in green. Produced with Molscript (35) and rendered with Raster3D (36). (*b*) The pH dependence of the k_{cat} and K_m values of *X. campestris* TDO. (*c*) The presence of L-Trp causes a large, positive shift in the reduction potential of TDO. SHE, standard hydrogen electrode.

final concentration) was included in the media for preparation of the holoenzyme samples (23). The protein was purified by using nickel-affinity and gel-filtration chromatography.

Point mutations were created with the QuikChange II site-directed mutagenesis kit (Stratagene, La Jolla, CA). The mutations and their associated ORFs were verified by DNA sequence analysis.

Protein Crystallization. To obtain the structure of TDO in the ferrous state, the protein was reduced by the addition of sodium dithionite, and all steps were performed in an anaerobic glove box (Belle Technology, Dorset, U.K.), with the O_2 concentration maintained <2 ppm. Excess sodium dithionite was removed by gel filtration (Sephadex G25 column) before crystallization. Crystals of TDO were grown by the sitting-drop vapor diffusion method with a well solution comprising 100 mM Mes (pH 6.3), 10–12% (wt/vol) PEG 4000, 60 mM $MnCl_2$, 10 mM sodium dithionite, and 2 mM L-Trp. Before mounting in nylon loops and flash-freezing in liquid nitrogen, crystals were immersed in a cryoprotectant solution composed of mother liquor (with L-Trp concentration increased to 50 mM) supplemented with 23% (vol/vol) glycerol and bubbled with nitric oxide for 15 min before use.

Data Collection and Processing. X-ray diffraction data were collected at the X4A beam line of National Synchrotron Light Source (Brookhaven National Laboratory, Upton, NY), the 21BM beam line at Advanced Photon Source (Argonne National Laboratory, Argonne, IL), and the BM14 beam line at the

Table 2. Summary of kinetic data on *X. campestris* TDO

Enzyme	Substrate	k_{cat}·(s^{-1})	K_m, μM	K_d Ferric heme, mM	K_d Ferrous heme, μM
Wild type					
	L-Trp	19.5 ± 1.2	114 ± 1	3.84 ± 0.14	4.12 ± 0.24
	D-Trp	0	16.5 mM ± 3.3*	>50†	NC
	6-F-D/L-Trp	37.3 ± 0.6	186 ± 12	2.45 ± 0.42	<1†
	5-F-D/L-Trp	2.40 ± 0.10	100 ± 6	1.51 ± 0.08	<1‡
	Indolepropionic acid	0	0	>10†	126 ± 11
	O_2§	35.4 ± 0.9	119 ± 2	0	NA
H55A mutant	L-Trp	2.86 ± 0.10	133 ± 7	ND	3.7 ± 1.3

NA, K_d for O_2 cannot be measured in the absence of substrate because of oxidation or in the presence of substrate because of turnover; NC, No spectral change detected; ND, not done.

*Inhibitory constant, K_i.

†Although a spectral change was evident, substrate solubility prevented accurate measurement of K_d. Values were estimated based on the maximum substrate concentration attainable.

‡Binding was too tight to be measured. Values quoted represent the minimum K_d that can be measured under standard assay conditions.

§The peak positions of the oxyferrous complex (O_2-TDO) are at 420 nm, 548 nm, and 578 nm.

BIOCHEMISTRY

European Synchrotron Radiation Facility (Grenoble, France). The diffraction images were processed and scaled with the HKL package (24). The data-processing statistics are summarized in Table 1, and more complete information can be found in SI Table 3.

Structure Determination and Refinement. The structures of the apo enzymes of TDO and SO4414 were determined by the selenomethionyl single-wavelength anomalous diffraction method (15). The selenium sites were located with SnB (25), and the reflection phases were calculated with Solve/Resolve (26). The structures of the holoenzymes and the ternary complex were determined by the molecular-replacement method, with the programs COMO (27) and AMoRe (28). The atomic models were built with the program XtalView (29) and TURBO-FRODO (30), and the structure refinement was carried out with CNS (31).

Electronic Spectroscopy, Steady-State Assays, and Dissociation Constant Measurements. Electronic absorption spectra were recorded by using a Cary 50-Probe UV-Visible spectrophotometer at 25°C. Assays for the steady-state turnover (at pH 7.5) of L-Trp and derivatives were performed as described (32, 33), except that substrate concentrations of 0–15 mM were used. The kinetic data were fitted to the Michaelis–Menten equation. The pH dependence of the steady-state kinetics was determined in the same manner, by using phosphate (pH 6.0–8.0) and Tris (pH 8.0–9.0) buffers. The electronic absorption spectra of the steady state were recorded by using a stopped-flow spectrophotometer (SX.17MV; Applied-Photophysics, Surrey, U.K.) in conjunction with a diode array detector, housed in an anaerobic glove box ($[O_2]$, <5 ppm; Belle Technology).

OTTLE Electrochemistry. Anaerobic potentiometric titrations were carried out as described (34) at 25°C by using a modified quartz EPR OTTLE cell. Titrations were performed in both the absence and presence of L-Trp (15 mM), and the heme reduction potentials were determined by fitting the data to the Nernst equation for a single-electron process by using Origin software (MicroCal, Northampton, MA). Reduction potentials are quoted versus the standard hydrogen electrode.

We thank Randy Abramowitz and John Schwanof at the National Synchrotron Light Source (Brookhaven National Laboratory, Upton, NY) and Hassan Belrhali at the European Synchrotron Radiation Facility (Grenoble, France) for setting up the beam lines and G. DeTitta of Hauptman Woodward Research Institute (Buffalo, NY) for crystallization screening. This research was supported by Grants P50 GM62413 and U54 GM074958 from the Protein Structure Initiative of the National Institutes of Health.

1. Yoshida R, Hayaishi O (1987) *Methods Enzymol* 142:188–195.
2. Takikawa O (2005) *Biochem Biophys Res Commun* 338:12–19.
3. Sono M, Roach MP, Coulter ED, Dawson JH (1996) *Chem Rev* 96:2841–2887.
4. Mellor A (2005) *Biochem Biophys Res Commun* 338:20–24.
5. Munn DH, Zhou M, Attwood JT, Bondarev I, Conway SJ, Marshall B, Brown C, Mellor AL (1998) *Science* 281:1191–1193.
6. Mellor AL, Munn DH (2004) *Nat Rev Immunol* 4:762–774.
7. Grohmann U, Fallarino F, Puccetti P (2003) *Trends Immunol* 24:242–248.
8. Uyttenhove C, Pilotte L, Theate I, Stroobant V, Colau D, Parmentier N, Boon T, van den Eynde BJ (2003) *Nat Med* 9:1269–1274.
9. Schwarcz R (2004) *Curr Opin Pharmacol* 4:12–17.
10. Muller AJ, DuHadaway JB, Donover PS, Sutanto-Ward E, Prendergast GC (2005) *Nat Med* 11:312–319.
11. Miller CL, Llenos IC, Dulay JR, Weis S (2006) *Brain Res* 1073–1074, 25–37.
12. Platten M, Ho PP, Youssef S, Fontoura P, Garren H, Hur EM, Gupta R, Lee LY, Kidd BA, Robinson WH, *et al.* (2005) *Science* 310:850–855.
13. Littlejohn TK, Takikawa O, Truscott RJW, Walker MJ (2003) *J Biol Chem* 278:29525–29531.
14. Sugimoto H, Oda S-I, Otsuki T, Hino T, Yoshida T, Shiro Y (2006) *Proc Natl Acad Sci USA* 103:2611–2616.
15. Hendrickson WA (1991) *Science* 254:51–58.
16. Daraselia N, Dernovoy D, Tian Y, Borodovsky M, Tatusov R, Tatusova T (2003) *OMICS* 7:171–175.
17. Holm L, Sander C (1993) *J Mol Biol* 233:123–138.
18. Cady SG, Sono M (1991) *Arch Biochem Biophys* 291:326–333.
19. Terentis AC, Thomas SR, Takikawa O, Littlejohn TK, Truscott RJW, Armstrong RS, Yeh S-R, Stocker R (2002) *J Biol Chem* 277:15788–15794.
20. Unno M, Matsui T, Chu GC, Couture M, Yoshida T, Rousseau DL, Olson JS, Ikeda-Saito M (2004) *J Biol Chem* 279:21055–21061.
21. Ishimura Y, Makino R, Iizuka T (1980) *Adv Enzyme Regul* 18:291–302.
22. Sono M (1989) *Biochem* 28:5400–5407.
23. Littlejohn TK, Takikawa O, Skylas D, Jamie JF, Walker MJ, Truscott RJW (2000) *Protein Expr Purif* 19:22–29.
24. Otwinowski Z, Minor W (1997) *Methods Enzymol* 276:307–326.
25. Weeks CM, Miller R (1999) *J Appl Crystallogr* 32:120–124.
26. Terwilliger TC (2003) *Methods Enzymol* 374:22–37.
27. Jogl G, Tao X, Xu Y, Tong L (2001) *Acta Crystallogr D* 57:1127–1134.
28. Navaza J (1994) *Acta Crystallogr A* 50:157–163.
29. McRee DE (1999) *J Struct Biol* 125:156–165.
30. Roussel A, Cambillau C (1991) *TURBO-FRODO. Silicon Graphics Geometry Partners Directory* 86 (Silicon Graphics, Mountain View, CA).
31. Brunger AT, Adams PD, Clore GM, DeLano WL, Gros P, Grosse-Kunstleve RW, Jiang J-S, Kuszewski J, Nilges M, Pannu NS, *et al.* (1998) *Acta Crystallogr D* 54:905–921.
32. Ishimura Y (1970) *Methods Enzymol* 17A:429–434.
33. Papadopoulou ND, Mewies M, McLean KJ, Seward HE, Svistunenko DA, Munro AW, Raven EL (2005) *Biochem* 44:14318–14328.
34. Ost TW, Clark JP, Anderson JLR, Yellowlees LJ, Daff S, Chapman SK (2004) *J Biol Chem* 279:48876–48882.
35. Kraulis PJ (1991) *J Appl Crystallogr* 24:946–950.
36. Merritt EA, Bacon DJ (1997) *Methods Enzymol* 277:505–524.